Available online at www.sciencedirect.com
SCIENCE DIRECT®

Journal of the European Ceramic Society 24 (2004) 763–773

www.elsevier.com/locate/jeurceramsoc

Mechanical behaviour of ferroelectric films on perovskite substrate

O. Bernard[a], M. Andrieux[a], S. Poissonnet[b], A.-M. Huntz[a,*]

[a]*LEMHE UMR 8647 CNRS Bâtiment 410 F-91405 Orsay, France*
[b]*SRMP CEA Saclay F-91 191 Gifsur Yvette, France*

Received 5 December 2002; received in revised form 7 April 2003; accepted 13 April 2003

Abstract

This paper is focused on the mechanical behaviour of single and multilayered ceramic systems on ceramic substrate. The ferroelectric ceramic PLT ($Pb_{0.9}La_{0.1}TiO_3$) was deposited using magnetron sputtering on (001) STO ($SrTiO_3$) and on a YBCO ($YBa_2Cu_3O_7$), as a 200 nm interlayer on STO. DRX and SEM observations were carried out to determine the microstructure of the various films, and TEM cross sections were realised to control the film thickness and grain epitaxial relationships. AFM was used as a roughness controller before and after deposition. Mechanical properties of the films and substrate were determined using micro and nanoindentation tests. Young's modulus and hardness of each system (STO, PLT/STO, YBCO/STO, PLT/YBCO/STO) were calculated and a peculiar phenomenon, associated to the YBCO interlayer addition, was observed. This work shows that YBCO improve mechanical properties of multilayered ceramics.

Keywords: Indentation; Mechanical properties; Perovskite; PLT/YBCOISTO; Thin films

1. Introduction

Ferro-electric films such as $Pb_{0.9}La_{0.1}TiO_3$ (PLT) are used in many industrial applications as field effect transistors (FETs), infrared sensors, ultrasonic sensors, etc... Their pyro and piezoelectric properties are well known. Microstructural properties and epitaxial relationships are well described as their fatigue and dielectric properties.[1–5] However, up to now, very few works deal with the mechanical properties of such films whereas hardness, toughness, adhesion of ferroelectric films must be taken into account for suitable industrial applications. Thus a great part of this work was focused on the mechanical properties of these films.

Mechanical properties were determined on two films with the same substrate $SrTiO_3$ (STO). The first system consists in PLT films on (001) STO single crystals, the second one in a PLT film deposited on an $YBa_2Cu_3O_7$ (YBCO) film deposited on (001) STO substrate. In order to understand the different results obtained on STO, the substrate and the YBCO film mechanical properties were also specified.

Our main objectives during this work were as it follows:

- Characterisation of the microstructure of the materials.
- Evaluation of hardness and Young's modulus of each film and substrate.
- Influence of the superconductor ceramic interlayer on the mechanical and adhesion properties of the film/interlayer/substrate system.
- Attempts at interpreting the observed mechanical phenomena.

2. Materials and experiments

In all cases, the STO substrates are (001) one side polished single crystals and each edge of the substrate is parallel with [010] or [100] directions.

Both PLT films were deposited by R.F. magnetron sputtering in LPGP (laboratoire de physique des gaz et des plasmas, Orsay, France) at 650 °C with 1.5% O_2 partial pressure in the plasma (1.5%). This oxygen partial

* Corresponding author. Tel.: +33-1-69-15-70-20; fax: +33-1-69-15-48-19.
E-mail address: am.huntz@lehme.u-psud.fr (A.-M. Huntz).

0955-2219/03/$ - see front matter © 2003 Elsevier Ltd. All rights reserved.
doi:10.1016/S0955-2219(03)00324-8

pressure ensures the best quality of the ferroelectric film in terms of electric properties and low roughness.

The YBCO films were deposited on STO by magnetron sputtering in CRYSTAL GmBH industries, at 670 °C under O_2 partial pressure. This film is deposited on a CeO_2 interlayer, 50 nm thick, which acts as a stress buffer and keying layer. Stoichiometry of YBCO was not controlled but T_c measured by the manufacturer is equal to 77 K.

To control the film orientation, XRD (X-ray diffraction) (Cu Kα1 $\lambda = 0.154056$ nm) was performed on each layer. Rocking Curve experiments were carried out to determine the crystalline quality of the different films. Atomic force microscope (AFM) was used to control the roughness of all the samples on a 2×2 μm^2 surface (IOTA, Orsay, France). The microstructure and the thickness of these films were determined by scanning electron microscopy (SEM, Cambridge) and transmission electron microscopy (TEM, Jeol 2000 EX). SEM and TEM observations were performed first to determine some of the surface and in core film properties (homogeneity, compactness, grain size, grain morphology, possible second phase precipitation, etc...).

Vickers micro-indentation (Shimadtzu) (square based pyramidal indenter) and Berkovitch nano-indentation (Nanotest 550, Micro-Materials Ltd) (triangular based pyramidal indenter) tests were our main investigating tools to determine the mechanical properties of both the coatings and the substrate. In each case, four different loads (150, 300, 500 and 1000 mN) were applied at room temperature during ten seconds on cleaned samples, the ridges of the Vickers diamond indenter being parallel to [100] direction (so called 0° Vickers indentation in this study). Ten prints were performed at these different loads and observed by SEM. Vickers indenter was also turned by 45° (so called 45° Vickers indentation), to control if cracks and damages were equivalent in both orientations.

In order to determine the Vickers hardness (H_v) of both substrate and coatings, Eq. (1) was used:

$$H_V = 1.89\frac{F}{d^2} \tag{1}$$

F is the applied force and d the diagonal of the Vickers print.

Assuming a Palmqvist type cracking, the toughness of the films was calculated using the Laugier's approach.[6,7] It considers that the stress intensity factor (K_c) which controls surface crack extension is insensitive to the form of the crack beneath the surface (Palmqvist or halfpenny) (Fig. 1) and both Hertzian and Vickers indentation techniques were compared for a range of engineering ceramics and were in good agreement with standard tests:

$$K_c = 0.0143 \times \left(\frac{E}{H_v}\right)^{2/3} \times \sqrt{\frac{a}{\ell}} \times \frac{F}{c^{3/2}} \tag{2}$$

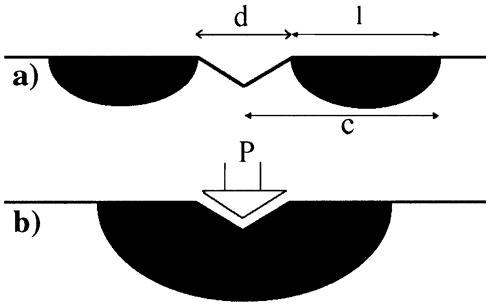

Fig. 1. Scheme of the two possible types of cracking: (a) Palmqvist type, (b) halfpenny type, according to Refs. 6 and 7.

with $a = d/2$, c the length of the cracks measured from the centre of the print, l the length of the cracks measured from the extremity of the print (Fig. 1), and F the applied load.

Anstis et al. approach was also used to determine the toughness of our ceramics coatings:[8,9]

$$K_c = 0.0154\left(\frac{E}{H_v}\right)^{1/2}\left(\frac{F}{c^{3/2}}\right) \tag{3}$$

Nano-indentation tests were made on all films. As for the micro-indentation tests, several indenter orientations were used to reveal or not an anisotropic mechanical response of the material. The Berkovitch indenter was turned of 0, 30 and 45° with regard to the [100] direction. Series of ten prints at four different penetration depths (100, 200, 500, 1000 nm) were realised in each configuration.

Using the technique proposed by Oliver and Pharr,[10,11] nano-indentation experiments allowed determining the hardness (H) and the Young's modulus (E) of every films and of the substrate. These values were used as references for K_c calculation.

Young's modulus E was calculated from the reduced modulus E_r determined by the apparatus using Eq. (4):

$$\frac{1}{E_r} = \frac{1-\upsilon^2}{E} + \frac{1-\upsilon_i^2}{E_i}$$
$$\text{with } \frac{1-\upsilon_i^2}{E_i} \text{ equal to } 8.710^{-4}\ \text{GPa}^{-1} \tag{4}$$

where v_i and E_i are the Poisson factor and the Young's modulus of the diamond of the indenter. Ten measurements at 100 nm were made for each nano-prints. It means ten load cycles with imposed penetration depth, the unloading part of the curves showing only the film elastic relaxation. Young's modulus was calculated using 80% of the unloading part of the curve and with $\varepsilon = 0.75$ (factor related to the punch geometry).

During indentation tests, an elastoplastic zone appears around the indenter. This affected zone must be included into the thickness of the film to determine available mechanical properties and values.

3. Results

3.1. Microstructure

Roughness of the surface and thickness of the different films are reported in Table 1. It shows the very low value of roughness of the substrate and of YBCO film. After deposition the surface roughness is superior to the substrate initial values but are of the same order of magnitude whatever the substrate on which PLT is deposited (i.e. STO or YBCO/CeO_2/STO). XRD experiments were managed on PLT/STO and reported in recent work.[12,13] PLT is (100) and (001) textured and rocking curves show the good long distance order of these films : the full width at half maximum, FWHM, is equal to 0.2°. YBCO film is textured around the [001] direction and reveals good epitaxial relationships with STO. Rocking curves (around the [005] direction) reveal the long-range order of this film, the FWHM is 0.78° without any deposited film and the FWHM is 0.69° after the PLT deposition. PLT deposited on YBCO/CeO_2/STO has a similar morphology and microstructure to PLT deposited on STO. YBCO interlayer does not affect the film characteristics. The XRD data are equivalent in this case to XRD data corresponding to PLT/STO. Only a little variation in the c parameter of YBCO is visible ($\delta c = 0.47\%$). This can be attributed to a variation in oxygen stoichiometry during PLT deposition.

SEM observations on YBCO films have shown an unvarying structure without any porosity. This film has a polycrystalline structure, but grain size estimation was not possible by SEM [Fig. 2 (a)]. The quality of the images could be affected by the insulator properties of the substrate. PLT films on STO present a vermicular structure and the porosity seems to be quite important [Fig. 2(b)]. This kind of microstructure could be the consequence of a 2D-3D growing mode of the film. Nevertheless this film was suitable for optical applications.[12] PLT films deposited on YBCO/STO present the same vermicular structure.

Thin foils of cross-section were realised on all systems. Results concerning PLT/STO were already discussed in Ref. 12: the ferroelectric PLT film presented a columnar structure and PLT grains were very often misoriented of 3° between them. For PLT/STO, three different orientation types were observed:

Table 1
Roughness of the surface and thickness of the different parts of the studied systems

	RMS (nm)	Thickness (nm)
STO	0.2	Thick sample
PLT/STO	8	550
YBCO + CeO_2/ STO	0.7	150 + 50
PLT/YBCO/STO	9	550/200

1. $(001)_{PLT}//(001)_{STO}$ $(100)_{PLT}//(100)_{STO}$,
2. $(010)_{PLT}//(001)_{STO}$ $(001)_{PLT}//(100)_{STO}$,
3. $(100)_{PLT}//(001)_{STO}$ $(010)_{PLT}//(100)_{STO}$,

the interface plane being (001).

Concerning the YBCO/CeO_2/STO system, it appears that the YBCO layer is 150 nm thick and very dense and homogeneous.[13] Orientation of the films compared to STO is reported below [Fig. 3 (a) and (b)]:

$(100)_{YBCO}//(100)_{STO}$ $(001)_{YBCO}//(001)_{STO}$
$(010)_{YBCO}//(010)_{STO}$, $(001)_{CeO2}//(001)_{STO}$
$(100)_{CeO2}(110)_{STO}$ $(010)_{CeO2}//(-110)_{STO}$.

The parametric mismatch *in the film plane* was calculated considering the previous epitaxial relationships, and taking for the parameters : $a_{STO} = 0.3905$ nm, $a_{YBCO} = 0.382$ nm, and $a_{CeO2} = 0.5411$ nm.

Thus

$$\delta_{CeO_2/STO} = \frac{a_{CeO_2} - a_{STO} \cdot \sqrt{2}}{a_{STO} \cdot \sqrt{2}} = -2\%$$

and

$$\delta_{YBCO/CeO_2} = \frac{a_{YBCO} \cdot \sqrt{2} - a_{CeO_2}}{a_{CeO_2}} = -0.16\%$$

The situation, considering that the different films are stress free (no matter continuity), is schematized in Fig. 3(c). When joining the interfaces, Fig. 3(d), it generates compressive stresses in CeO_2 near the interface with YBCO and tensile stresses in CeO_2 near the interface with STO. As already mentioned by authors,[14,15] the intermediate CeO_2 layer has a strain buffer function and decreases the stress level between the ferroelectric film and the substrate. As a consequence, shear stresses are minimised and mechanical adhesion is enhanced. As said before, PLT deposited on YBCO/CeO_2/STO has a similar microstructure than that of PLT deposited on STO. Fig. 3(e) is a micrograph relative to a transverse thin foil of PLT/YBCO/CeO_2/STO observed by TEM. It shows the quality of the multilayered system. PLT is made up of columnar grains with twins (white areas into the columnar grains), and it can be verified that the microstructure of YBCO is not modified by the PLT film deposition. By comparison with previous studies,[12,13] it can be observed that the PLT growth is similar whatever the substrate, i.e. STO or YBCO/CeO_2/STO and similar epitaxial relationships are detected [Fig. 3(f)]:

$(001)_{PLT}//(001)_{YBCO}$ $(100)_{PLT}//(100)_{YBCO}$,
$(001)_{YBCO}//(001)_{CeO_2}$ $(110)_{YBCO}//(100)_{CeO_2}$,
$(001)_{CeO_2}//(100)_{STO}$ $(100)_{CeO_2}//(011)_{STO}$.

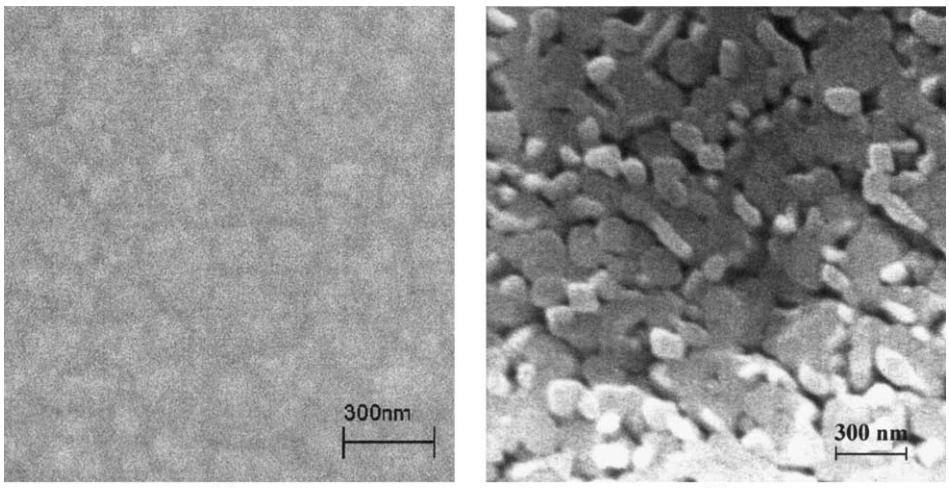

Fig. 2. SEM observations: (a) YBCO surface, (b) PLT/STO surface.

The deposition process leads to *c*-axis PLT on either STO or YBCO. According to the various values of the parameters: $a_{PLT} = 0.395$ nm, $c_{PLT} = 0.406$ nm, $a_{YBCO} = 0.382$ nm and $a_{STO} = 0.3905$ nm, the parametric mismatch can be calculated as previously. It leads to the following small values: $\delta_{PLT/STO} = 1.15\%$ and $\delta_{PLT/YBCO} = 2.2\%$.

3.2. Micro and nano indentation

3.2.1. STO

During Vickers micro-indentation tests, cracks and cleavage appeared at different loadings i.e. at different depths. This allows having a good appreciation of the substrate damages. For 0° Vickers indentations, cracks always appears perpendicularly to the print's sides and their number increases proportionally to the loading. It means that the cracks always propagate along to the [110] directions of the substrate as shown in Fig. 4(a). It is important to observe that all prints are square shaped, which denotes the mechanical isotropy of this material and presence of deformation zones perpendicular to the print's diagonals can also be observed; these deformation zones are "rosette" and can be sometimes observed during indentation tests.[16] The different parts of the rosette arms have all the same direction [100] or [010]. The rosette dimension increases with the loading, and for a load of 500 mN [Fig. 4(b)] in micro-indentation, the rosette grows to become a square with cracks in the diagonals. Strain and damages do not remain localised but extend with increasing the load. When turning the indenter of 45°, cracks appear this time at the corners of the prints, in the same direction [110] as in the case of 0° prints. Now there is no multi-cracking configurations, each corner of the indenter giving rise to only one crack [Fig. 5 (a)]. Lot of steps parallel to the prints sides are now visible [Fig. 5(b)], when it was not the case with the 0° prints. These steps form a sort of pile-up around the print. To control the presence or not of a pile-up formation, optical interferometer was used. It shows that for a print diagonal of 20 μm (load of 1000 mN) the pile-up is 500 nm high (Fig. 6).

Nano-indentation prints show no significant differences according to the orientation of the indenter. During these tests, pop-in and cracks apparition are visible on the load vs. penetration depth curves (Fig. 7). Pop-in phenomena correspond to the little steps on the loading part of the curve. Nevertheless, cracks always appear along [110]. There is formation of a non-symmetric pile-up (with regard to the print symmetry) around the nano prints for a determined level of strain (Fig. 8). The print is triangular and the pile up seems to be a square.

3.2.2. YBCO/CeO_2/STO

A very interesting phenomenon appears for Vickers prints at the minimal load (150 mN) at 45°; it consists in the presence of cracks along [110] direction (as for STO), and cracks perpendicular to the prints side along [100] direction (Fig. 9). For this loading, buckling is also visible around the print. When the applied force rises, buckling increases and the shape of the print seems to be equivalent with prints realised on STO; there is a pile-up formation around the print, and the presence of the steps in the spalled zones is visible (Fig. 10). For small depth prints (100 nm), the spalled zone around the indenter is not triangular but square shaped (Fig. 11). When increasing the penetration depth, cracks appear around the print and on the ridges of the prints and there are lots of spalled region; but in this case the crack propagation is not systematically along a [110] direction. For highest depth penetration (400 and 800 nm), a large part of the substrate is uncoated beside the prints. Pop-in rarely appears during loading, just one or two little steps on 800 nm depth loading curves.

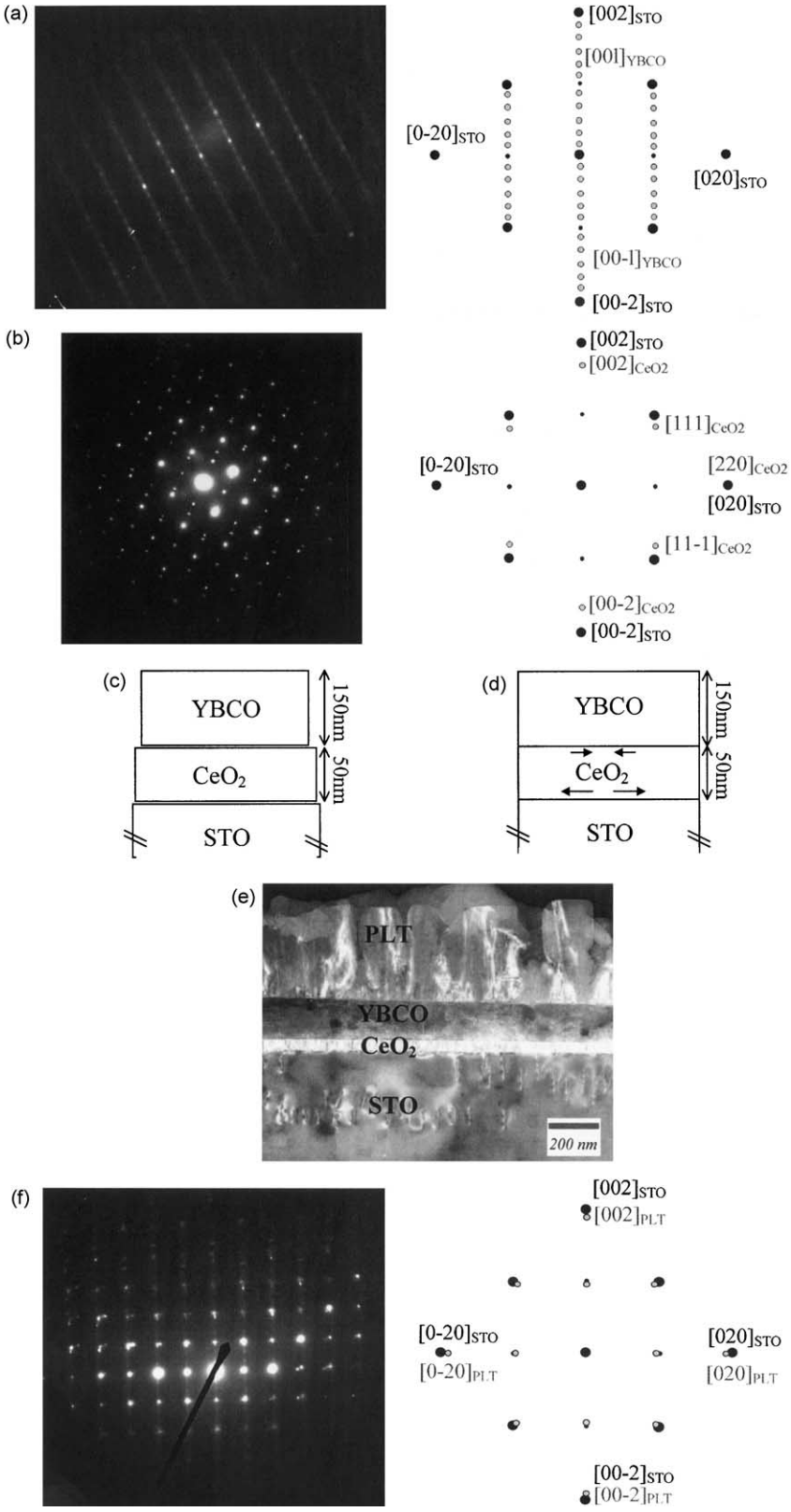

Fig. 3. Transmission electron microscopy on PLT–YBCO–CeO_2–STO system: (a) diffraction pattern of YBCO/STO, (b) diffraction pattern of CeO_2/STO, (c) schematic representation of the stress free system (d) schematic representation of compressive and tensile strains in CeO_2 interlayer when joining the layers, (e) observation (TEM) of the PLT/YBCO/CeO_2/STO thin foil, (f) diffraction pattern of PLT/YBCO/CeO_2/STO.

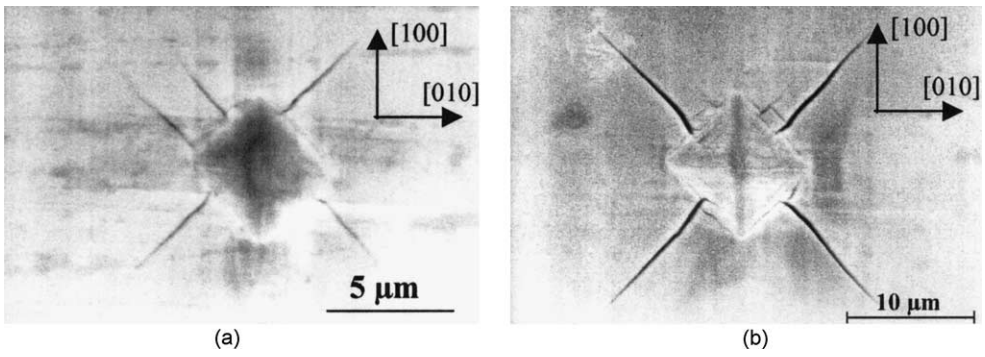

Fig. 4. Vickers prints on STO: (a) 150 mN 0°, (b) 500mN, 0°.

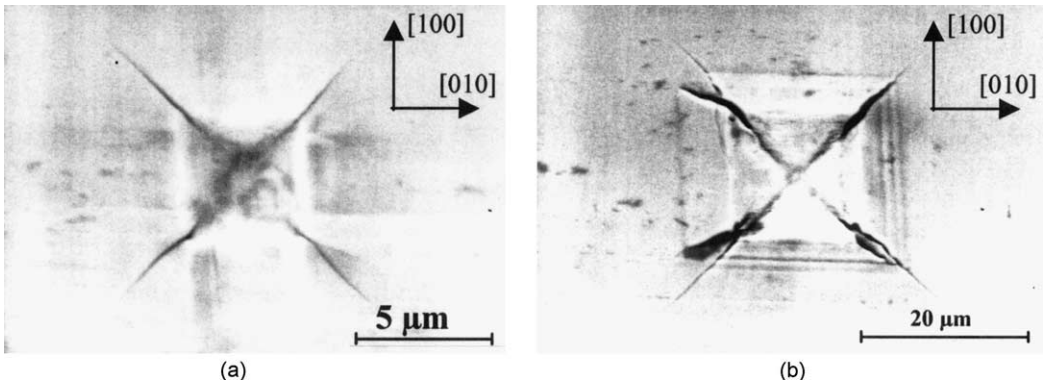

Fig. 5. Vickers prints on STO: (a) 150 mN, 45°, (b) 1000 mN, 45°.

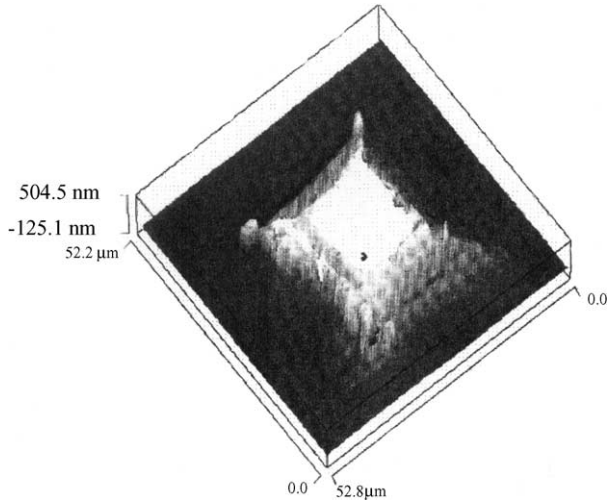

Fig. 6. Interferometric image of a pile up around a 1000 mN 45° Vickers print.

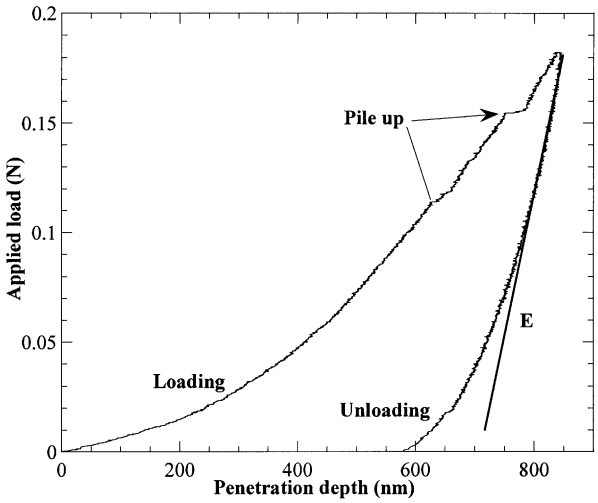

Fig. 7. Representation of a loading-unloading nano indentation curve, with the Pop-in effect and elastic relaxation on the unloading part of the curve.

3.2.3. PLT/STO

For PLT/STO films, when the minimal load is applied (150 mN), little cracks appear in the corners of the prints without visible buckling. Buckling appears between 150 and 300 mN and the buckled region is always circular (Fig. 12). In many cases, cracks delimit the stick up region. It is particularly visible for high loads (1000 mN). In all cases, cracks parallel to the prints sides appear on the buckled film, as if the film was pushed up and pressed in the direction of the print. Buckled surfaces are equal for a given load and cracks distribution is uniform. Spalling of the film appears between 500 and 1000 mN, and spalled surfaces are not equivalent. The vermicular structure of the film do not permit to visualise the cracks in the film during nano-indentation tests, but there is a pile up formation around the prints and lots of spalled zones for penetration depth

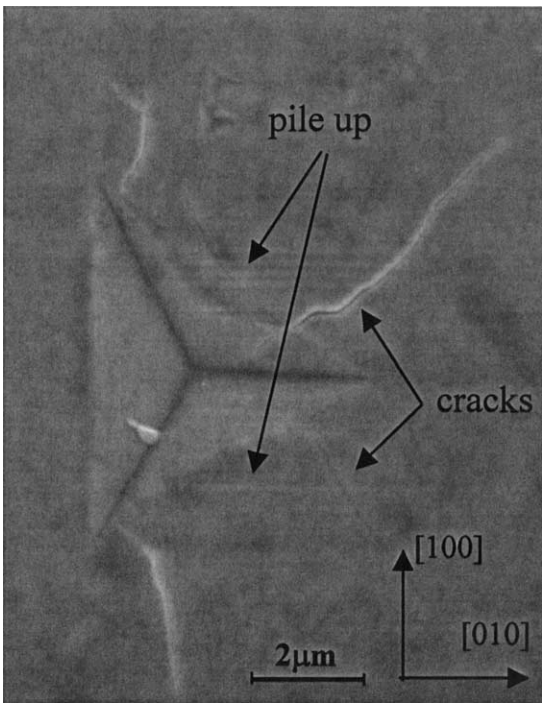

Fig. 8. SEM image of a Berkovitch nano print (800 nm, depth 0°) on STO with pile-up formation (parallel lines).

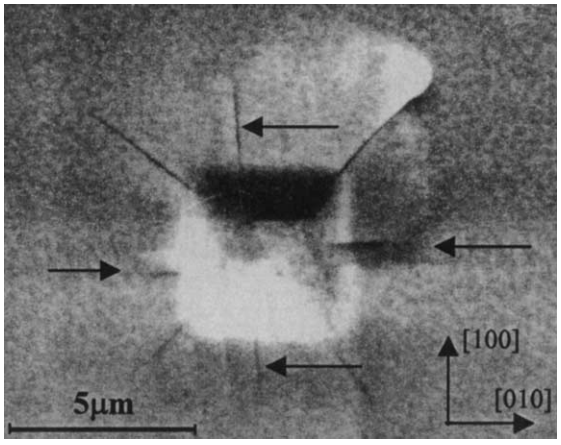

Fig. 9. Vickers print at 150 mN, 45°, on YBCO/STO showing the peculiar cracking mode of the coating.

superior or equal to 800 nm. Pop-In is also quite important during loading for 800 nm depth prints.

3.2.4. PLT/YBCO/CeO_2/STO

With the adjunction of YBCO (200 nm) interlayer, no cracks are visible for 150 and 300 mN and first cracks appear for 500 mN or less. Buckling certainly appears between 300 and 500 mN. As for PLT/STO case, cracks delimit the buckled region but, compared to the previous case, the loading limit for buckling is two times higher. Crack apparition is delayed by the YBCO interlayer and loading required for crack apparition is now two or three times greater than for PLT directly on STO (Fig. 13).

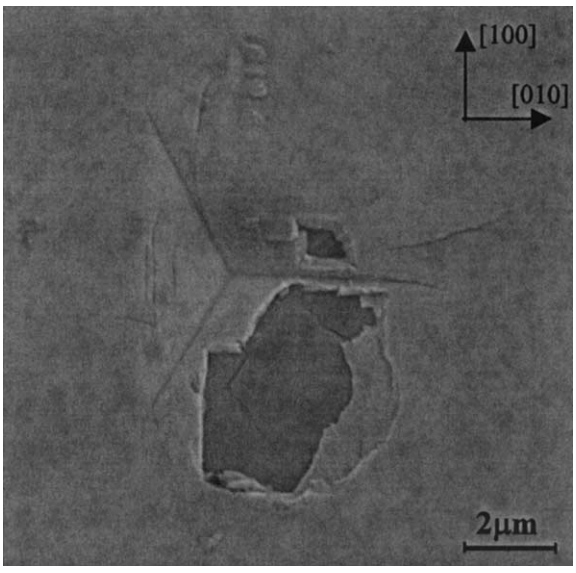

Fig. 10. SEM image of a Berkovitch nano print, at 800 nm indentation depth, on YBCO/STO with large spalled zone.

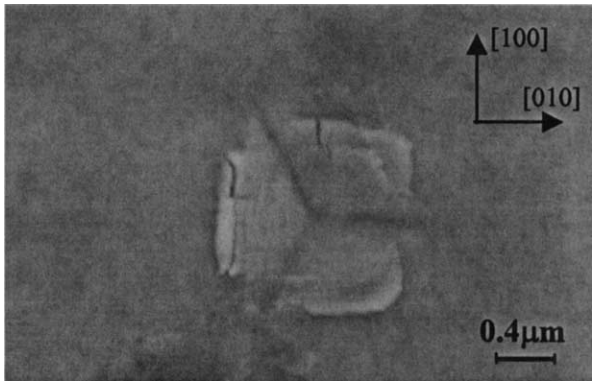

Fig. 11. SEM image of a Berkovitch nano print, at 100 nm indentation depth, on YBCO/STO.

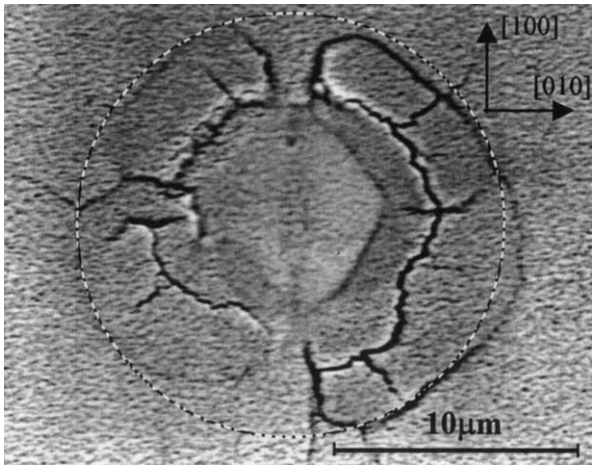

Fig. 12. SEM image of a Vickers print, at 500 mN, 0°, on PLT/STO showing the circular buckled zone (back scattering electron mode: BSE).

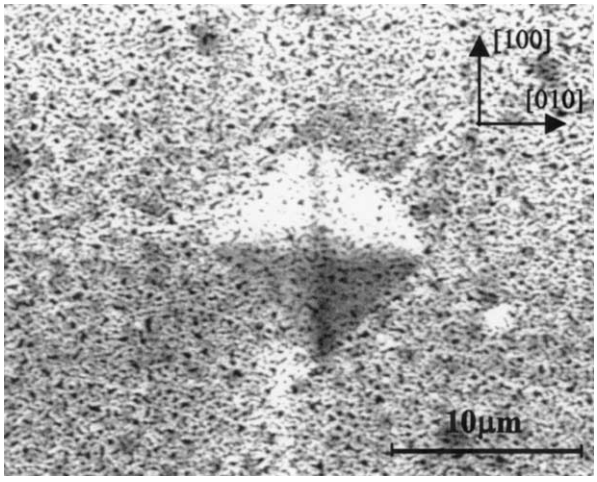

Fig. 13. SEM image of a Vickers print, at 500 mN, 0°, on PLT/YBCO/STO: note that there is no buckled zone and cracks (Back scattering electron mode: BSE).

As in PLT/STO case, the cracks are not visible and piles-up around the prints are detected without any spalled zones. There is no pop-in during loading in most of cases, only a pop-in effect was observed for 550 nm depth on the loading curve during performing 800 nm depth prints.

3.3. Mechanical characteristics

Hardness of the substrate (STO) was first estimated with Vickers micro-indenter. Indeed, during these experiments, when a crack appears, there is a mechanical relaxation in the material. As a consequence, the penetration depth is more important than expected and the measured hardness is so underestimated. Fig. 14 presents the evolution of hardness as a function of load (i.e. inversely proportional to the print diagonal). For high penetration depths, lots of cracks imply that calculated hardness is very low. Conversely, for low penetration depths, the hardness value tends to the bulk one, around 7.5 GPa.

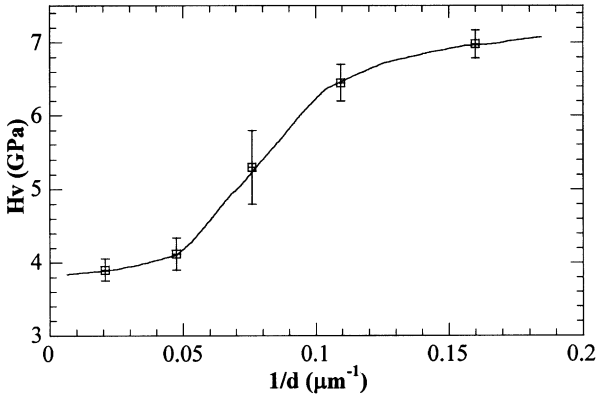

Fig. 14. Evolution of Vickers micro-hardness on STO as a function of the load, thus inversely proportional to the print diagonal.

The values of hardness and Young's modulus of the different systems were determined with Berkovitch nano-indentation for low penetration depths and are reported in Fig. 15 and in Table 2. In that case, cracks in our brittle materials are avoided. Hardness value of of 9.5 GPa for the bulk STO was determined whereas YBCO/CeO_2/STO value reaches 12.5 GPa. For higher penetration depths (500 or 1000 nm, i.e. five times the film thickness) hardness of the film is logically equivalent to the substrate. Hardness of PLT film (6.4 GPa) on STO is inferior to STO hardness (9.5 GPa).

One can notice that hardness of the films are very different from one to another, YBCO is the hardest with 12.5 GPa and STO is harder than PLT with 9.5 GPa versus 6.4 GPa for the ferroelectric film.

Young's modulus of the films and substrate are very close with a general value of 230 GPa. Substrate's toughness was calculated with the two models presented above [Eqs. (2) and (3)] and both give a value of 1 ± 0.1 MPam$^{0.5}$. This toughness value is comparable to glass, silica, MgO and many oxides.[17]

4. Discussion

Microstructural experiments have shown the good quality of the various PLT films, in terms of controlled

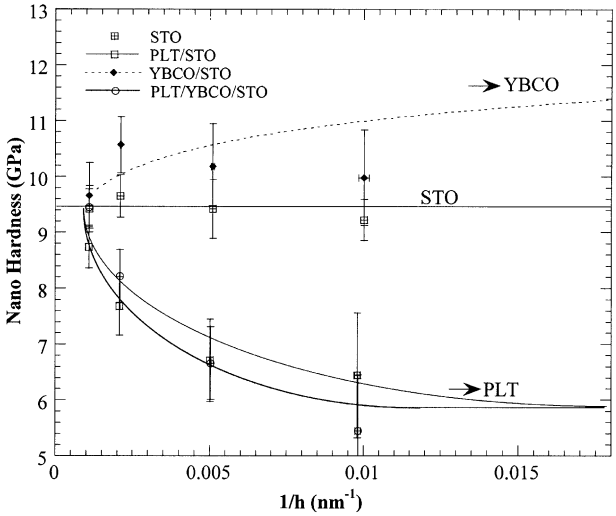

Fig. 15. Evolution of the nano-hardness of the different coating systems as a function of the inverse of the indentation depth.

Table 2
Young modulus and hardness (average value) determined on the different components of the layers for low penetration depths by nano-indentation

	Young's modulus (GPa)	Hardness (GPa)	E/H
$SrTiO_3$	225±14	9.5±1.3	23.7±1.7
$YBa_2Cu_3O_7$	235±20	12.5±2.5	18.8±2.2
$Pb_{0.9}La_{0.1}TiO_3$	185±40	6.4±1.0	29.4±1.7

epitaxy and compactness of the ferro-electric film. The roughness and the vermicular structure of the PLT film did not change when introducing or not an YBCO interlayer. All these results suggest that the physical properties of the PLT film are equivalent when deposited on STO or on YBCO/CeO_2/STO.

From mechanical considerations, Young's moduli determined on the different components are slightly equivalent, certainly due to the fact that the films and the substrate are both perovskite (i.e. their structural properties are very closed).

Micro-indentation tests show the specific cracking mode of the substrate, cracks around the Vickers prints are always along [110] directions. By turning the indenter by 45°, it is observed that the corners are not the cracks promoters. Increasing the loading induces the formation of a specific pile-up around the Vickers print which can reach 500 nm for an applied load of 1000 mN (cf. Fig. 6). Observations suggest that such piles-up are a consequence of a specific gliding system around the print, in the (011) and (101) planes. Recent work dealing with compression tests on STO at room temperature reveals plastic strain, with a comparable gliding system (1-10) [110].[18] An equivalent behaviour during indentation was reported on MgO.[19] Interstitial loops with a [001] burgers vector are generated during indentation. Then, the loops tend to adopt a square form to dissociate in two dislocations with [110] burgers vector lying in (110) planes. These dislocations are glissile in these planes, then during indentation the dislocations reach the surface and lead to steps which can be observed. In STO, (110) planes are dense planes and recent results reported by Gumbsch et al.[18] shows a low temperature plasticity carried by [110](1-10) dislocations. This mechanism can explain the easiness of pile-up formation and the extension of radial cracks around 45° Vickers prints with the increasing applied load [cf. Fig. 5(b)]. Only the crack part included in the deformation zone has its width increased. Crack apparition is certainly the consequence of a dislocation recombination as in MgO case:[19]

$$\frac{1}{2}a\left[01\bar{1}\right]+\frac{1}{2}a\left[\bar{1}01\right]=\frac{1}{2}a\left[\bar{1}10\right]$$

But now the slip plane is not {110} type but {112} type so that the two glissile dislocations recombination leads to a sessile dislocation formation. So, during indentation tests, there is formation of glissile and sessile dislocations leading to stress concentration and finally crack formation in {110}-type plane, which bisects the intersecting slip planes.

During nanoindentation tests, cracks appear around the berkovitch prints and always along [110] direction. This shows that the punch geometry is not the cause of [110] cracks apparition. STO cracks develop along [110] and pilling-up grows parallel to the print's sides. As a consequence, the kind of fracture along [100] and [010], revealed in Figs. 9 and 11, is proper to YBCO film. For higher loads, these secondary cracks disappear and are only visible inside the prints: the primary cracks only subsist, and sticking off is important. All these facts show the mechanical action of STO during indentation. For a peculiar loading limit, STO imposes his own deformation pattern and cracking mode. On the other hand, the cracks propagate in YBCO and the pilling up formation release the YBCO coating.

Calculation of films hardness was realised with nano-indentation tests because the elastoplastic sphere around the micro-indenter is too large to only determine the films mechanical characteristics. Low PLT hardness value can be attributed to the vermicular structure of the film for many reasons: a bad position of the punch at the start (in a pore for example), cracks apparition during the tests in coalescence zones and not visible in the loading curve. But the calculated hardness is equivalent in every indenter configuration for the PLT/STO and PLT/YBCO/CeO_2/STO systems; this hardness value (6.4 GPa ± 1.0 GPa) should be a good estimate of this PLT film. Higher hardness value of YBCO can be explained by the compactness of this layer and perhaps the internal compressive stresses, as observed by Bai et al.[20] on CN_x films on (111) Si. Compressive stress field offers a resistance to indenter penetration so that the measured penetration depth is lower and the calculated hardness appears artificially higher than it is really. For high penetration tests, hardness of the single layer system tends to the substrate hardness because the film mechanical effect is hidden by the substrate one.

For low penetration depth (small load), the indentor is only affected by the mechanical behaviour of the PLT film. As shown by Fig. 15, the PLT hardness (6.4 GPa) is similar whatever the layers on which it is deposited and is representative of the film alone. It was also observed that the loading and unloading curves obtained by nano-indentation for low penetration depth on PLT/STO and on PLT/YBCO/STO look accurately like the same. It demonstrates that the mechanical characteristics of the PLT films are similar.[20] However, structural, microstructural or stress level modification could affect hardness measurements. In our case, as there are no differences concerning the hardness, the structure and the microstructure of PLT films according to the nature of the substrate (deposited either on STO or YBCO/STO), the stress level of the PLT film on YBCO/CeO_2/STO should be equivalent to the stress level of the PLT film on STO.

When using microindentation tests, the effect of the YBCO interlayer on the mechanical adherence and resistance of PLT film is obvious on all tests. For the same penetration depth, PLT film damages are reduced

and crack density is lower than without YBCO (Figs. 12 and 13). As mechanical properties of PLT are similar whatever the substrate, the YBCO interlayer must play the role of a strain buffer layer. No specific observations could show the true mechanical role of the interface, but there is clearly an effect of the YBCO interlayer on the adhesion of the PLT film. However, it is difficult to define the part of YBCO which interferes with the elastoplastic zone created by the indentor and modifies the hardness measurements (complex stress distribution around interfaces). Thus, in order to understand the differences in the mechanical behaviour of the PLT film during indentation and the damages that can be observed without an intermediate YBCO layer, the Burnett and Rickerby approach based on the E to H ratio was used[21] to estimate the plastic zone areas for the same load in each considered case. The low strain transfer between PLT and STO could explain buckling (in PLT/STO) system [Fig. 16(a)]. Indeed, it indicates that the strain transfer is very sharp at the interface and the generated shear stresses will be very important. As the E/H ratio is inferior for YBCO, the plastic strain sphere in the STO substrate is expected to be larger [Fig. 16(b)]: the strain continuity is promoted leading to smaller shear stresses. For the PLT/YBCO/STO system, the join of both interface effect [Fig. 16(c)] leads to a better adhesion of the system.

Using the same approach, the effect of the YBCO interlayer is also visible when the loading curves at 800 nm depths are compared for the different coating systems (Fig. 17). Pop-in effect is also affected by this interlayer addition. This Pop-in effect on PLT/STO loading curves is reduced on YBCO/CeO_2/STO's one, and there is only a little pop-in effect at 750 nm for PLT/YBCO/CeO_2/STO (which corresponds to the PLT + YBCO thickness). The small plastic zone drawn on Fig. 16(a) generates high stress concentration. As a consequence, pop-in appears for very low penetration depth. Conversely, when the plastic zone is bigger (YBCO/STO system), stress concentration is lower and pop-in appears for higher penetration depth [Fig. 16(b)]. When considering the both films (PLT/YBCO/STO system), the superimposition of the two plastic zones improves the mechanical behavior, probably by offsetting the PLT/STO system effect. Pop-in appears for very high penetration depth in comparison with the others systems (Fig. 17). Pop-in decreasing leads to a decrease in pile-up growing in STO (described above). The cracks and spalled zones apparition is delayed too. For an equivalent load the adhesion of PLT is improved.

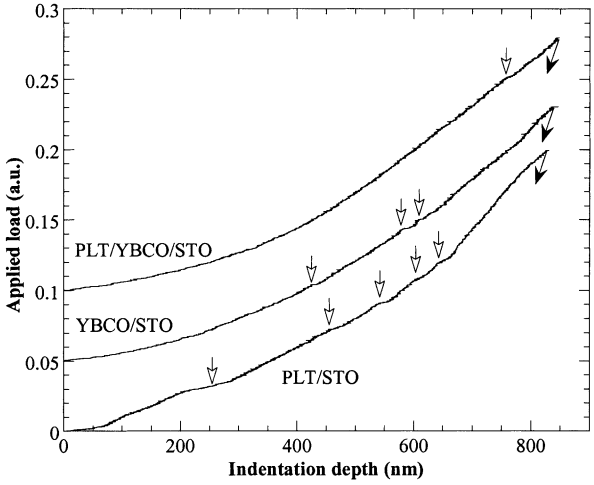

Fig. 17. Comparison of loading curves at 800 nm penetration for the three different coating systems. White arrows represent pop-in effect. Note that, on PLT/STO, five large "pop-in" are visible while three are visible on YBCO/CeO_2/STO and only one on PLT/YBCO/CeO_2/STO.

5. Conclusions

All the microstructural experiments showed that the structure of the PLT film is the same whatever the substrate, with or without YBCO interlayer: physical properties of the PLT films in term of permittivity and mechanical properties which are closely connected to the microstructure do not differ. Micro and nano-indentation tests show the peculiar mechanical response during indentation of the STO substrate and give some data on single crystal perovskite hardness values and information on the deformation mode. Film's hardness and Young's modulus were determined and YBCO interlayer shows its positive action for decreasing the cracks density and spalling during indentation tests. An interpretation of these phenomenons can be given using Burnett-Rickerby approach and the pop-in reduction with the superconductive interlayer addition is another evidence of the better mechanical behaviour of the PLT/YBCO/CeO_2/STO system.

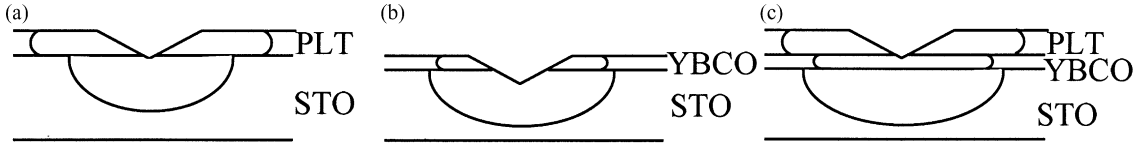

Fig. 16. Schematic representation of the mechanical affected zone for the: (a) PLT/STO system, (b) YBCO/CeO_2/STO system, (c) PLT/YBCO/CeO_2/STO system.

Acknowledgements

This work was supported by an ACIB of the french research ministery. Moreover, the authors are indebted to J. M. Desvignes, U. Rabibisoa, M. C. Hugon for elaborating the PLT films, to C. Haut for his help in microscopy and to B. Poumellec who allows to use the interferometric microscope.

References

1. Speck, J. S. and Pompe, W., Domain configurations due to multiple misfit relaxation mechanisms in epitaxial ferroelectric thin films. I. Theory. *J. Appl. Phys*., 1994, **76**(1), 466–476.
2. Foster, C. M., Pompe, W., Daykin, A. C. and Speck, J. S., Relative coherency strain and phase transformation history in epitaxial ferroelectric thin films. *J. Appl. Phys*., 1996, **79**(3), 1405–1415.
3. Hideaki, Adachi, Tsueno, Mitsuyu, Osamu, Yamazaki and Kiyotaka, Wasa, Ferroelectric (Pb,La)(Zr,Ti)O_3 epitaxial thin films on sapphire grown by rf-planar magnetron sputtering. *J. Appl. Phys*., 1986, **60**(2), 736–741.
4. Young Min, Kang, Ja Kang, Ku and Sunggi, Baik, Crystallographic characterization of tetragonal (Pb,La)TiO_3 epitaxial thin films grown by pulsed laser deposition. *J. Appl. Phys*., 1995, **78**(4), 2601–2606.
5. Seong Jun, Kang, Dong Hoon, Chang and Yung Sup, Yoon, Fatigue and dielectric properties of the (Pb,La)TiO_3 thin films with various La concentrations. *Thin Solid Films*, 2000, **373**, 53–59.
6. Laugier, M. T., Indentation testing of engineering ceramics and cermets. *Nuclear Science Technology Section in European Applied Research Reports*, 1987, **7**, 1171–1182.
7. Laugier, M. T., New formula for indentation toughness in ceramics. *J. Mat. Sci. Lett*., 1987, **6**, 355–358.
8. Anstis, G. R., Chantikul, P., Lawn, B. R. and Marshall, D. B., A critical evaluation of indentation techniques for measuring fracture toughness. I. Direct crack measurements. *J. Am. Ceram. Soc*., 1981, **64**, 533–538.
9. Anstis, G. R., Chantikul, P., Lawn, B. R. and Marshall, D. B., A critical evaluation of indentation techniques for measuring fracture toughness. II. Strength method. *J. Am. Ceram. Soc*., 1981, **64**, 539–543.
10. Oliver, W. C. and Pharr, G. M., *Mechanical Properties and Deformation Behaviour of Materials having Ultra-fine Microstructures*. Kluwer Academic Publishers, 1993.
11. Oliver, W. C. and Pharr, G. M., An improved technique for determining hardness and elastic modulus using load and displacement sensing indentation experiments. *J. Mater. Res*., 1992, **7**(6), 1564–1583.
12. Rabibisoa, U., Aubert, P., Bridou, F., Hugon, M. C. and Agius, B., Epitaxial growth of (Pb,La)TiO_3 thin films on (0001) Al_2O_3 and (001) $SrTiO_3$ substrates by RF magnetron sputtering. *Ferroelectrics*, 1999, **225**(1-4), 303–310.
13. Bernard, O., Poulat, S., Poissonnet, S., Huntz, A. M. and Andrieux, M., Mechanical behaviour of a multilayer system for microelectronic applications. *Proceeding TFDOM-2, J.Phys. IV France*, 2001, **11**(Pr 11), 35–39.
14. Wu, X. D., Foltyn, S. R., Townsend, J., Adams, C., Campbell, I. H., Tiwari, P., Coulter, Y. and Peterson, D. E., High current $YBa_2Cu_3O_{7-\delta}$ thick films on flexible nickel substrates with textured buffer layers. *Appl. Phys. Lett*., 1994, **65**(15), 1961–1963.
15. Ovsyannikov, G. A., Mashtakov, A. D., Mozhaev, P. B., Komissinskii, F. V., Ivanov, Z. G. and Larsen, P., Improvement of the conducting parameters of $YBa_2Cu_3O_x$ films grown on sapphire through the use of strontium titanate buffer layer. *Technical Physics Letters*, 1998, **24**(9), 676–678.
16. Woirgard, J., Tromas, C., Girard, J. C. and Audurier, V., Study of the mechanical properties of ceramic materials by the nanoindentation technique. *J. Eur. Ceram. Soc*., 1998, **18**, 2297–2305.
17. Schutze, M.. In *Protective Oxide Films and Their Breakdown*, ed. D. R. Holmes. The Institute of Corrosion and Wiley series on corrosion and protection, Chichester, UK, 1991.
18. Gumbsch, P., Taeri-Baghbadrani, S., Brunner, D., Sigle, W. and Rühle, M., Plasticity and an inverse brittle-to-ductile transition in strontium titanate. *Phys. Rev. Lett*, 2001, **87**(8) (085505-1-085505-4)..
19. Khasgiwal, N. and Chan, H. M., High-temperature indentation studies on the {110} plane of single-crystal magnesium oxide. *J. Am. Ceram. Soc*., 1992, **75**(6), 1924–1928.
20. Bai, M., Kato, K., Umehara, N. and Miyake, Y., Nanoindentation and FEM study of the effect of internal stress on micro/nano mechanical property of thin CN_x films. *Thin Solid Films*, 2000, **377-378**, 138–147.
21. Burnett, P. J. and Rickerby, D. S., Assessment of coating hardness. *Surface Engineering*, 1987, **3**(1), 69–76.